Predictability of the Barents Sea ice cover from the sea surface temperatures in a linear framework

Aleksi Nummelin[1], Chuncheng Guo[2], and Patrik Bohlinger[3]

[1]University of Oslo
[2]NORCE Norwegian Research Centre, Bjerknes Centre for Climate Research
[3]The Norwegian Meteorological Institute

November 23, 2022

Abstract

The Barents Sea attracts year-around human activity as the winter sea ice cover retreats, creating a need for short and long term prediction of environmental conditions in the region. Previous studies have shown that local ocean heat content and heat transport at the Barents Sea Opening provide interannual to decadal predictability of Barents Sea ice cover. Part of this predictability is suggested to originate from thermodynamic anomalies propagating along the Norwegian Atlantic Current. To better understand this source of predictability, and the relevant timescales, we use models (Coupled Model Intercomparison Project Phase 6; CMIP6) and satellite observations, to study the linear response of the monthly mean Barents Sea ice cover to downstream sea surface temperature anomalies. We show that in March the sea ice response is strongest on short lead times (<2 year), vanishing towards ˜7 year timescale and that the linear sea ice response function can be reconstructed using an advective-diffusive 'leaky-pipe' model with multiple propagation timescales. The sea surface temperature based sea ice predictability is linked to decadal and longer timescale variability. Our results also show that sea surface temperatures close to the sea ice edge provide the best predictability at short timescales, but with a skill that approaches that of the sea surface temperatures further away at long timescales.

Predictability of the Barents Sea ice cover from the sea surface temperatures in a linear framework

Aleksi Nummelin[1], Chuncheng Guo[1], and Patrik Bohlinger[2]

[1]NORCE Norwegian Research Centre AS and Bjerknes Centre for Climate Research
[2]Norwegian Meteorological Institute

Key Points:

- Monthly mean Barents Sea ice cover responds to upstream ocean temperatures within a 7 year timescale.
- The CMIP6 mean sea ice response function can be represented using multiple anomaly propagation speeds in a 'leaky-pipe' model.
- The linear response functions provide weak predictability of the March Barents sea ice concentration in climate models.

Corresponding author: Aleksi Nummelin, `aleksi.h.nummelin@gmail.com`

Abstract

The Barents Sea attracts year-around human activity as the winter sea ice cover retreats, creating a need for short and long term prediction of environmental conditions in the region. Previous studies have shown that local ocean heat content and heat transport at the Barents Sea Opening provide interannual to decadal predictability of Barents Sea ice cover. Part of this predictability is suggested to originate from thermodynamic anomalies propagating along the Norwegian Atlantic Current. To better understand this source of predictability, and the relevant timescales, we use models (Coupled Model Intercomparison Project Phase 6; CMIP6) and satellite observations, to study the linear response of the monthly mean Barents Sea ice cover to downstream sea surface temperature anomalies. We show that in March the sea ice response is strongest on short lead times (<2 year), vanishing towards ~ 7 year timescale and that the linear sea ice response function can be reconstructed using an advective-diffusive 'leaky-pipe' model with multiple propagation timescales. The sea surface temperature based sea ice predictability is linked to decadal and longer timescale variability. Our results also show that sea surface temperatures close to the sea ice edge provide the best predictability at short timescales, but with a skill that approaches that of the sea surface temperatures further away at long timescales.

Plain Language Summary

The Barents Sea attracts year-around human activity as the winter sea ice cover retreats, creating a need for short and long term prediction of environmental conditions in the region. Previous studies have shown that ocean temperatures can be used to predict Barents Sea sea ice area years ahead suggesting that changes in ocean temperatures move from south to north along the Norwegian coast. We use climate models and satellite observations to better understand this source of predictability. We show that the monthly sea ice response in winter is strongest on short lead times (<2 year) and vanishes after ~ 7 years from a change in the ocean temperatures. We also find that the predictability, even at short timescales, is due to variability at $\sim$10 year and longer timescale and that the relationship is strongest close to the sea ice edge.

1 Introduction

Predictions of Barents Sea ice cover are crucial for year-round operations in the region that is an important marine habitat and hosts large natural resources from fish stocks to oil-and-gas fields. Previously, both observations and models have shown that the ocean heat transport to the Barents, and the heat content of the Barents Sea, are both good predictors for the winter ice cover in the region at interannual timescales (Årthun et al., 2012; Onarheim et al., 2015; Årthun & Eldevik, 2016; Årthun et al., 2017). At the same time, there could be potential to extend this predictability as both observations and models show that there are sea surface height and temperature anomalies that seemingly propagate along the Norwegian Atlantic Current from at least as far as the Greenland Scotland Ridge on a timescale of several years (with a speed of 1-2 cm/s; Furevik, 2000; Skagseth et al., 2008; Chepurin & Carton, 2012; Broomé & Nilsson, 2018; Årthun & Eldevik, 2016; Årthun et al., 2017; Muilwijk et al., 2018, and Fig. 1).

The idea of using upstream ocean observations to predict downstream evolution in environmental conditions along the Norwegian Atlantic Current as such is not new (see e.g. Helland-Hansen & Nansen, 1909), and the process understanding of the propagation mechanisms behind the predictable anomalies has been discussed ever since. Possible mechanism include both anomaly propagation as an oceanic mode (Broomé & Nilsson, 2018) and as a coupled atmosphere-ocean mixed layer mode (Nilsson, 2000). Most recently, oceanic propagation in the boundary current with lateral mixing has been shown to provide results that are qualitatively similar to observations (Broomé & Nilsson, 2018).

To better understand the propagation mechanisms and to quantify the associated predictability, we examine how the monthly Barents Sea ice cover co-varies with the upstream ocean conditions in CMIP6 models and in observations. Specifically, we will use the stochastic climate model paradigm of Hasselmann (1976) and assume that the Barents Sea ice cover (C; concentration) can be represented by a convolution of a (unknown) response function G and the (known) forcing history F:

$$C(t) = \int_0^{\tau_{max}} G(\tau)F(t-\tau)d\tau + \epsilon. \tag{1}$$

Where F are the upstream ocean conditions i.e. the SST anomalies at given sections along the Norwegian Atlantic Current (Fig. 1), τ is a time lag, τ_{max} is a maximum time lag, and ϵ is an error term. Writing (1) in an matrix form gives:

$$\boldsymbol{C} = \boldsymbol{G} \cdot \boldsymbol{F} + \boldsymbol{\epsilon}, \tag{2}$$

and allows us to solve for an estimate of $\boldsymbol{G}$ through regression (omitting the error term):

$$\hat{\boldsymbol{G}} = \boldsymbol{C} \cdot \boldsymbol{F}^{-1}. \tag{3}$$

Where the hat implies that we only solve for a statistical estimate of the true $\boldsymbol{G}$, and the negative exponent marks a matrix inverse. The stochastic climate model paradigm has been successfully used for prediction of many aspects of the climate system (Kostov et al., 2017, 2018; Johnson et al., 2018; Seviour et al., 2019; Lambert et al., 2019; Cornish et al., 2020). One of the main advantages of the methodology over naive lagged regression, is the response function $\boldsymbol{G}$ which provides a direct link to the dynamics governing the system - given that the the underlying covariances reflect causal relations.

The manuscript is structured as follows: we describe the data and methodology used in this study in section 2, we analyse the co-variability of sea ice concentration and sea surface temperatures in the CMIP6 models in section 3.1, we invert the sea ice concentration response functions in section 3.2, compare them to theory in section 3.3, and use the response functions together with SST anomalies to reconstruct and predict sea ice concentration anomalies in section 3.4. Finally, in section 4 we summarize and discuss the results in a broader context.

2 Data and Methods

In order to gain robust estimates of the response function $\boldsymbol{G}$ we will use long pre-industrial coupled climate model simulations from the Coupled Model Intercomparison Project phase 6 (CMIP6). Although previous studies have often focused on the ocean heat transport as a predictor for the Barents Sea ice cover, we will use sea surface temperature (SST) as a predictor. Using SST is a pragmatic choice that allows using a much larger number of CMIP6 models as well as allowing for comparison to satellite observations (Reynolds et al., 2007). We acknowledge that we are limited in predictive capability since the heat transport is a function of both temperature and volume transport, and it is really the heat transport convergence that enters the heat content equation that ultimately impacts sea ice formation. Not accounting for the volume transport variability is likely to decrease the skill of the prediction

We will use (3) to solve for $\hat{\boldsymbol{G}}$. Following Johnson et al. (2018) we take $\boldsymbol{C}$ to be the sea ice concentration timeseries (vector of length N; the length of the timeseries in years) for a given month and $\boldsymbol{F}$ the lagged SST forcing history (matrix of size $N \times \tau_{max}$). All values are detrended and de-seasonalized by removing the monthly average values for each month and then normalized by dividing by their (monthly) standard deviations.

Similar to Johnson et al. (2018) we form an ensemble of $\hat{\boldsymbol{G}}$s by dividing the full SST timeseries of length N to overlapping segments of length τ_{max} and by varying τ_{max} between 2-10 years in 12 month increments (resulting in N_{max} different response functions).

This procedure gives us a matrix of response functions for each model with dimensions ($\tau_m ax$, N/τ_{max}, N_{max}). To construct a response function that is robust to over-fitting to a particular time period, we take the median over the two last dimensions.

3 Results

3.1 Timescales of variability in CMIP6 models

We focus our analysis on March which is when the observed Barents Sea ice area peaks. In March, the CMIP6 models show a large spread in both mean and variability of the Barents Sea SIC and the Nordic Seas SSTs (Figs. 1a and 2a). The lagged correlation analysis suggest that the Barents Sea SIC is (inversely) linked to upstream SSTs with decreasing correlation (Fig. 1a) and increasing lag (Fig. 1b) when moving away from the sea ice edge along the Norwegian coast.

Figure 2a shows that both the Barents Sea SIC and upstream SST spectra are red, peaking at multidecadal timescales, with increasing ensemble spread towards the long timescales. Similar dominance of long timescales in the region has been previously demonstrated by e.g Årthun & Eldevik (2016) who found an approximately 14 year timescale for Nordic Seas temperature variability in the observations and somewhat wider range (10-20 years) of variability in CMIP5 models.

The CMIP6 median coherence between the upstream sea surface temperatures and Barents Sea ice cover suggest that at 0-lag most of the co-variability takes place at the decadal and longer timescales (Fig. 4b). There is also a notable increase in coherence, especially at decadal timescales, when moving from the southern Nordic Seas to close to the Barents Sea Opening.

Given the long timescales of variability, and the fact that the coherence is largest at long timescales, we expect that most of the predictability coming out of the response functions is also linked to the long timescales.

3.2 Reconstructed Response Functions

We use (3) to invert for the response function $\hat{\boldsymbol{G}}$ in 30 CMIP6 models (Table S1) and in the satellite observations (OI-SST, 1982-2019; Reynolds et al., 2007). As expected, the response functions reflect the multiple timescales seen in the timeseries analysis (Figs. 3 and S1). Most models have strong weights for the first few months (lags), but then for some models (e.g CESM2 variants) the $\hat{\boldsymbol{G}}$ reaches zero at $\sim$2-3 year lags, whereas others (e.g. NorESM2 variants) show close to constant weights for the first 4-5 year lags before reaching zero at around 6-7 year lags (Fig. S1). In the northernmost sections the OI-SST (satellite observations) based response function lies within the CMIP6 response functions for the first $\sim$ 4 year lags. However, further south and at longer lags the OI-SST response function becomes increasingly noisy, which we attribute to the short observational record, and eventually departs from the CMIP6 ensemble.

The wide spread among the CMIP6 models is clear in the step response (integral of the response function, Fig. 3b). The CMIP6 median shows that in the absence of any other forcing, the sea ice response to instantaneous 1 standard deviation perturbation in SST at 72°N leads to 0.6 standard deviation perturbation in sea ice concentration within $\sim$5 years. Although it is unclear if the OI-SST based response function is robust at long lags, it suggests that there is a net positive response between 5-9 year lags, possibly indicating a secondary feedback from the sea ice to the sea surface temperatures. The CMIP6 mean response does not show such behaviour, but some individual models (gray lines in Fig. 3) do.

In general there is only a small decrease in the CMIP6 response functions when moving further away from the sea ice edge (Figs. 3, S1). However, especially in the models with a response function dominated by short timescales, the response function is the strongest for the sections that are closest to the ice edge. In models where long timescales are pronounced, the different sections have similar response functions. The CMIP6 median suggest that the integrated sea ice response is ∼0.4 STD for a 1 STD SST perturbation in the Greenland-Scotland ridge, but ∼0.6 STD for a 1 STD SST perturbation in the Barents Sea Opening. Our analysis here has focused on March, but the response functions for other winter months are similar (Fig. S2).

3.3 Comparison to Theoretical Response Functions

Theoretical response functions based on anomaly propagation in a diffusive ocean (e.g. Jeffress & Haine, 2014; Broomé & Nilsson, 2018, , so called 'leaky-pipe' model) or in an atmosphere-ocean mixed layer mode (e.g Nilsson, 2000) suggest that a SST anomaly that is initially a delta function, has an imprint of a widening Gaussian function with a decaying amplitude as one moves further away from the source. In reality the situation is more complex; at any given time an anomaly consists of contributions from a multitude of signals due to variability at different timescales. In addition, between two locations there are a number of different processes that propagate an anomaly forward (see e.g. Sundby & Drinkwater, 2007; Lien & Vikebø, 2014; Chafik et al., 2015; Asbjørnsen et al., 2019; Broomé et al., 2020, for discussion on remote and locally generated anomalies). Therefore, we propose that instead of representing one propagating anomaly between the target section and the Barents Sea, the reconstructed response functions represent the envelope that a multitude of Gaussian functions create.

Here we will demonstrate such behavior with the response function for the leaky pipe-model, which simulates anomaly propagation in an advective-diffusive system that is connected to a large heat reservoir. Such a system could be the boundary current - deep basin system imagined here following (Broomé & Nilsson, 2018), but with a different set of parameter values the same model could represent the atmosphere - ocean mixed layer system, for example. The asymptotic form (assuming large distances and lead times) of the response function for the leaky-pipe model is (slightly rewritten from Broomé & Nilsson, 2018)

$$G_{lp} = \underbrace{\sqrt{\frac{a\epsilon}{4L_c\pi\tau}}\exp\left(\frac{2ax}{L_r}\right)}_{A}\sqrt{u_e}\exp\left(-\frac{a\tau^2u_e^2+ax^2}{L_ru_e\tau}\right), \tag{4}$$

where the parameters are as follow: L_c is the width of the advective current (pipe), L_r is the reservoir width and ϵ is their ratio, $\epsilon = L_c/L_r$. u_e is the effective velocity of the anomalies (not the underlying advective velocity) and a is its relation to a eddy velocity v_e i.e. we take the two to be linearly related $v_e = au_e$ and choose $a = 1$ so that faster anomalies are also more diffusive. Finally, τ is the time lag and x is the distance from the source. To define the envelope of multiple Gaussian functions we find those u_e that lead to the largest G_{lp}. This can be done by solving when the u_e derivative of (4) is 0. Before going forward we note this derivative would have a much simpler form without the $\sqrt{u_e}$ term in (4). As we will see, removing this additional u_e dependency will also provide better match with the CMIP6 median response, and therefore we will further assume that G_{lp} has an additional u_e dependency of the form $B/\sqrt{u_e}$ (where B is a constant). A relevant physical argument is that the atmosphere (fast propagator, large u_e) dampens the SST anomalies more effectively than the ocean (slow propagator, small u_e). With these assumptions, the u_e derivative of (4) becomes

$$\frac{\partial G_{lp}}{\partial u_e} = -\frac{aAB(\tau u_e - x)(\tau u_e + x)\exp\left(\frac{ax^2}{L_r\tau u_e} - \frac{a\tau u_e}{L_r}\right)}{L_r\tau u_e^2}, \tag{5}$$

where A refers to the group of variables in (4). Ignoring the trivial solutions, $\frac{\partial G_{lp}}{\partial u_e} = 0$ when $\tau u_e - x = 0$ gives

$$u_e = x/\tau. \tag{6}$$

Note that by keeping the $\sqrt{u_e}$ term in (4) will require solving a quadratic equation to find u_e such that $\frac{\partial G_{lp}}{\partial u_e} = 0$. The solution to that quadratic equation becomes (negative root is not plausible)

$$u_e = \frac{L_r}{4a\tau} + \frac{\sqrt{L_r^2\tau^2 + (4a\tau x)^2}}{4a\tau^2}. \tag{7}$$

Substituting (6) or (7) to (4) then defines the envelope of multiple Gaussian functions representing signals that propagate at different speeds. In order to connect the SST anomalies propagating in the leaky-pipe model to the sea ice concentration, we assume that the sea ice concentration would be linearly related to the SST anomalies and allow for an additional coefficient in front of the Green's function in (4). In the following we then fit the upper and lower limits for the propagation speeds together with the constant connecting SST to the Barents Sea ice concentration.

Figure 4 shows a comparison between CMIP6 results and the leaky-pipe model with different velocities representing fast and slow propagation of anomalies. Note that the theoretical envelopes derived above return the maximum for each τ (dashed lines in Fig. 4), but as seen from Figure 4, the fitted models suggest that CMIP6 based Green's functions are best explained with a lower limit of 1 cm/s for the anomaly propagation, consistent with previous studies (Broomé & Nilsson, 2018). The upper limit suggested by the fit is not robust as it increases with the distance and at the same time the fits at short lags get gradually worse as one moves southward in the Nordic Seas. Nevertheless, the Green's functions suggest that only relatively fast propagation can explain the response function weights at short lags.

Based on our results it remains unclear if the fast propagation at short lags is due to SST anomaly propagation or due to a spatially coherent atmospheric forcing. However, the correlation structure at short lags (Fig. 1) is more in line with anomaly propagation along the Norwegian Atlantic Current than what one would expect for spatially coherent forcing. Therefore, we suggest that the anomaly propagation at least takes place at short lags, even if spatially coherent forcing might also contribute to the large weights.

Finally, we note that the heat transport based response functions for two models suggests a dominating propagation at 4-5 year timescale with a Gaussian like imprint on top of the SST response function like smooth envelope (Fig. S3).

Our next step (section 3.4) is to use the estimated response function $\hat{\boldsymbol{G}}$ to reconstruct the original timeseries $\boldsymbol{C}$. It is important to realize that even though the response functions show large weights on annual (<1 year lag) and inter-annual (1-5 year lag) timescales, we do not necessarily expect that those timescales would be well reconstructed. A response function reflects the relationship between a predictor and a predictant, but if the relationship is weak relative to all the other influences at a given timescale, the reconstruction can still be poor.

3.4 Hindcasts and Prediction

We use (2) with the estimated response function $\hat{\boldsymbol{G}}$ and the known forcing (SST at the different sections) to estimate the original sea ice concentration timeseries (hindcast). As suggested by the analysis in section 3.1 the reconstruction captures the long timescales well, but struggles to represent the short timescales (Fig. 5). In most models, and in the CMIP6 mean, essentially none of the SIC variability at timescales shorter than $\sim$10 years is captured by the SST based reconstruction.

Whereas in the hindcasting the forcing (SST) history is known up to zero lag, for predictability purposes we are interested in a longer predictability window i.e. lags that are greater than zero. The predictability depends on both the unknown future values of the predictor as well as the response function which links the time evolution of the predictor to that of the predictant. The naive approach is to use the response function with a zero-padded timeseries of the predictor or to assume that the last value persists to the future. However, a straightforward extension is to formulate a statistical model for the unknown future values of the predictor as well. Here, in addition to the naive approaches, we use a simple Gaussian process model to estimate the future values of SST given its historical (observed/simulated) values (Appendix A).

The prediction of the simulated sea ice with the model based response functions shows a slow decay in explained variance as the lag increases and one moves away from the sea ice edge (Fig. 6). There is a considerable spread among models and the distribution is skewed towards high skill. Although the response function based prediction outperforms the lagged regression at short lags and especially away from the sea ice edge, the persistence of the sea ice concentration itself is the best predictor for the fist 2 years. The differences between the SST prediction methods are relatively small for the first two years, after which the skill of the Gaussian process model based prediction quickly deteriorates. Both SST persistence and lagged regression show a seasonal signal, most likely due to summer SST anomalies being worse measures for the upper ocean heat content than the winter SST anomalies.

4 Summary and Discussion

We have shown that in the CMIP6 ensemble the Barents Sea ice cover responds to upstream ocean conditions within $\sim$7 year timescale, with the strongest response within the first $\sim$2 years. Close to the sea ice edge, this response is remarkably similar in the satellite observations and in the CMIP6 multimodel mean. The linkage between SST and the sea ice cover is strongest close to the ice edge, and translates to moderate predictability in the CMIP6 models ($r^2 \sim 0.3$ for the first $\sim$3 years, Fig. 6).

Our analysis of the spectral properties, together with the response functions, suggest that although the timescales that link the SSTs and sea ice together are short, the predictability is linked to decadal and longer timescales. Essentially, it is the short delay in the emergence of these long timescale signals between southern and northern Nordic Seas that provide the predictability.

In section 3.3 we have shown that allowing for multiple speeds in a 'leaky-pipe' model (Jeffress & Haine, 2014; Broomé & Nilsson, 2018) an advective-diffusive propagation can explain the shape of the CMIP6 median response functions. Although the parameters for the leaky-pipe model in this work are inspired by the ocean, the model itself can be modified to represent e.g. atmosphere - ocean mixed layer anomaly propagation. Therefore, we do not take the leaky-pipe fit to be definitive support for the dominance of the oceanic anomaly propagation, but rather we want to emphasize that instead of a single Gaussian like Green's function as in idealized systems, in the realistic systems there are multiple processes acting to propagate anomalies and therefore an envelope of Gaussians provides a better approximation to the reconstructed Green's functions.

Previous studies have shown that the short term variability of the Barents Sea ice cover is linked to the atmospheric variability, and the ice export from the Arctic proper to the Barents Sea. For operational purposes one could use a statistical model that extend the SST based response functions we have presented with a model that takes into account the short term atmospheric forcing (see also Onarheim et al., 2015). It is also likely that within one model system, or in observations, one could design more targeted

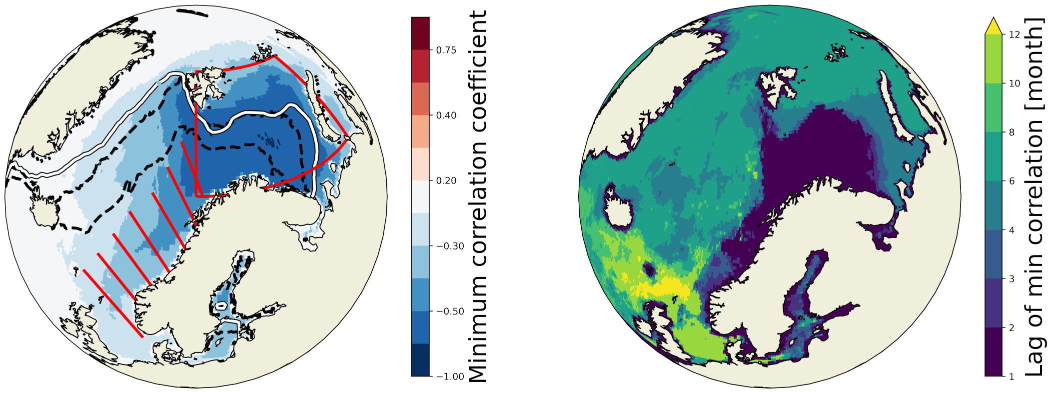

Figure 1. Lagged correlation between Barents Sea ice concentration and local SST in CMIP6 pre-industrial control simulations. Shading in panel a) shows the minimum correlation coefficient across 1-12 month lags whereas shading in panel b) shows at which lag the minimum correlation coefficient is found. Zero lag is omitted here, because it is uninteresting in terms of prediction. In panel a) we also show i) mean observed sea ice extent (1982-2019) in white, ii) 25% and 75% quartiles of the sea ice extent from the CMIP6 pre-industrial control simulations in black dashed contours, iii) Averaging region for the Barents Sea (used later in this study) as a red box, and iv) seven sections along the Norwegian coast that are used for averaging the sea surface temperatures that we use as a predictor for the sea ice conditions. Note that the average is taken over a 1° wide band centered at each section, and the sections are centered at every second latitude between approximately 60N and 72N (sections are defined in a rotated coordinate system in order to have sections perpendicular to the coast). In the text and in the other figures we refer to these sections by their (approximate) latitude.

sections than we did here, that would give more skilful SST based prediction of the ice cover.

Appendix A Gaussian Process model

We utilize a simple Gaussian Process (GP) model to model the predictor time series and assume that we are dealing with a zero mean process which has random but smooth changes with a certain degree of memory. The fact that the predictor variable is SST anomalies supports the assumption of a zero mean process. The GP model used here is described in detail in Bohlinger et al. (2019). We assume that the SST anomalies (hereafter referred to as y) are following a zero mean multivariate Gaussian distribution $y \sim N(0, \Sigma)$ with a covariance matrix $\Sigma = K + \sigma_n^2 I$, where Gaussian noise ($\sigma_n$) is added to the diagonals of the covariance matrix K that stems from the GP. We parameterize K with the following squared exponential kernel function (SE):

$$cov(y_t, y_{t'}) = \sigma_s^2 \exp\left(-\frac{(t-t')^2}{2l^2}\right) \tag{A1}$$

The SE kernel has the parameters σ_s and l which represent the signal variance and the length scale of the process, respectively. σ_s, σ_n, and l are learned and optimized based on the input data utilizing gradient descent. We put constraints on l to values between 3 and 10 years to reduce the influence of short term signals and increase the weights on longer time scales. The GP is more thoroughly described in Rasmussen & Williams (2006)

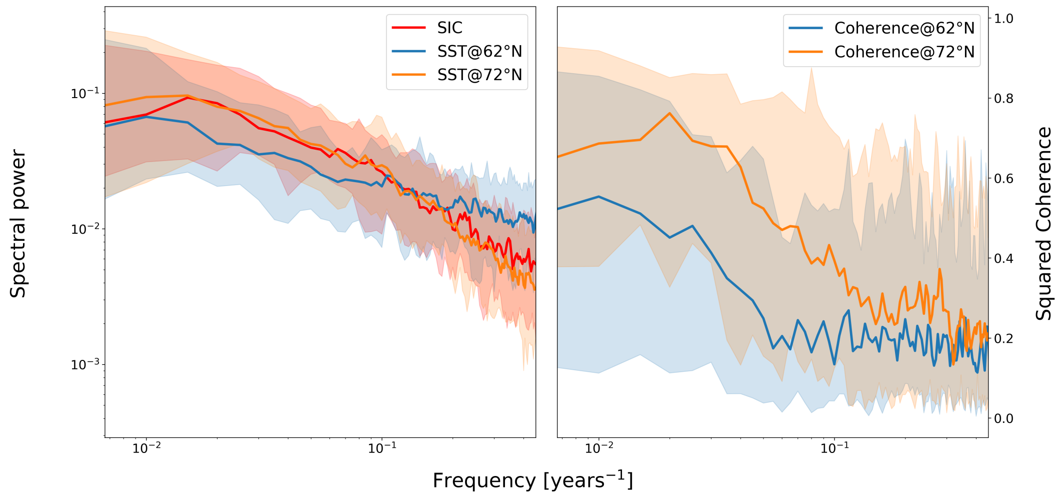

Figure 2. Spectral properties and coherence of the Barents Sea ice cover and the upstream ocean conditions. (a) Spectral power of normalized (by standard deviation) sea ice concentration (SIC) and sea surface temperature (SST) at northernmost and southernmost sections shown in Figure 1 (b) the spectral coherence between SIC and the SST at the respective sections. Solid lines show the median over the CMIP6 ensemble, whereas the shading shows the 5%-95% range.

and was recently applied for the purpose of time series modelling in Bohlinger et al. (2019) and**?** for the above described configuration. For convenience, we used the scikit-learn implementation (Pedregosa et al., 2011).

Acknowledgments

We acknowledge the World Climate Research Programme, which, through its Working Group on Coupled Modelling, coordinated and promoted CMIP6. We thank the climate modeling groups for producing and making available their model output, the Earth System Grid Federation (ESGF) for archiving the data and providing access, and the multiple funding agencies who support CMIP6 and ESGF. All the CMIP6 data used here is available through ESGF and the links to the data are given in Table S1. NOAA High Resolution SST (OI-SST) data is provided by the NOAA/OAR/ESRL PSL, Boulder, Colorado, USA, from their website at https://psl.noaa.gov/data/gridded/data.noaa.oisst.v2.highres.html.

References

Årthun, M., & Eldevik, T. (2016, 01). On Anomalous Ocean Heat Transport toward the Arctic and Associated Climate Predictability. *Journal of Climate*, *29*(2), 689-704. Retrieved from `https://doi.org/10.1175/JCLI-D-15-0448.1` doi: 10.1175/JCLI-D-15-0448.1

Årthun, M., Eldevik, T., Smedsrud, L. H., Skagseth, Ø., & Ingvaldsen, R. B. (2012, 07). Quantifying the Influence of Atlantic Heat on Barents Sea Ice Variability and Retreat*. *Journal of Climate*, *25*(13), 4736-4743. Retrieved from `https://doi.org/10.1175/JCLI-D-11-00466.1` doi: 10.1175/JCLI-D-11-00466.1

Årthun, M., Eldevik, T., Viste, E., Drange, H., Furevik, T., Johnson, H. L., & Keenlyside, N. S. (2017, Jun 20). Skillful prediction of northern climate provided by the ocean. *Nature Communications*, *8*(1), 15875. Retrieved from `https://doi.org/10.1038/ncomms15875` doi: 10.1038/ncomms15875

Asbjørnsen, H., Årthun, M., Skagseth, Ø., & Eldevik, T. (2019). Mechanisms of

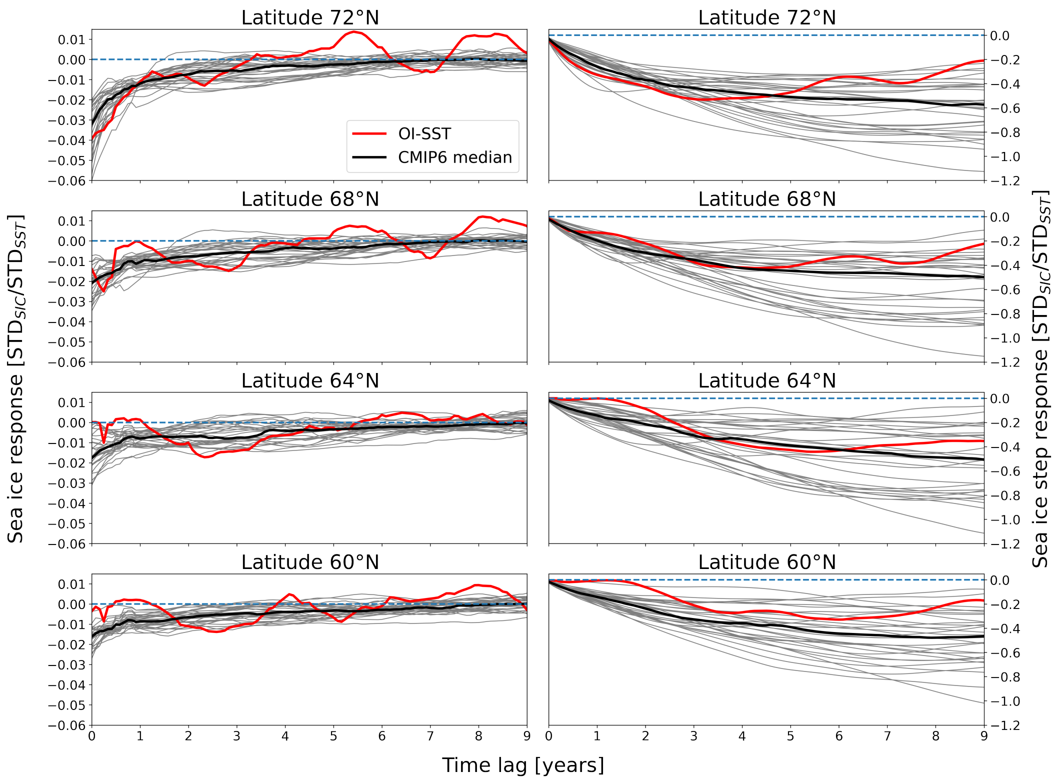

Figure 3. Barents Sea SIC response function to the mean SST at different sections along the Norwegian Atlantic Current on the left and their integrals i.e. response to SST delta function at time 0 on the right. The gray lines in the background show the individual CMIP6 models, the red line shows the satellite observations (OI-SST), and the black line shows the CMIP6 ensemble median. Note that prior to solving for the response function all values are normalized by their standard deviation (STD) and therefore the response functions have units of $[STD_{SIC)}/STD_{SST}]$ i.e. if SST changes by 1 STD, the response function shows the SIC response in STD_{SIC}.

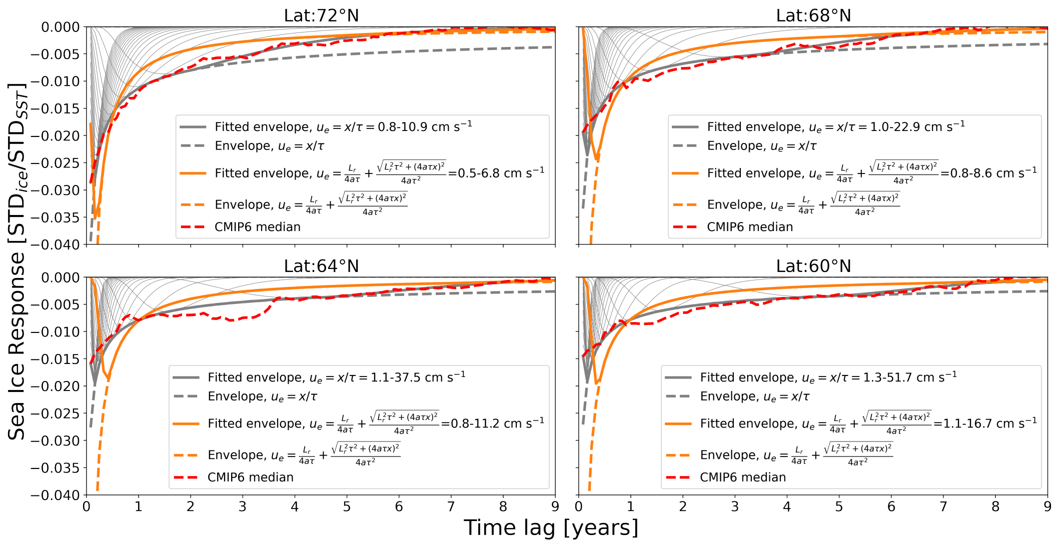

Figure 4. Leaky-pipe model envelope and CMIP6 median Barents Sea SIC response function to SST at different sections along the Norwegian Atlantic Current. The thin gray lines in the background show the individual leaky-pipe predictions with different propagation speeds. The theoretical envelopes (dashed, gray and orange) show the envelope without any constraints on the propagation speed, whereas the fitted lines (solid gray and orange) show the envelopes when the propagation speed is fitted so that the envelope best matches the CMIP6 median (the speed range is included in the label)

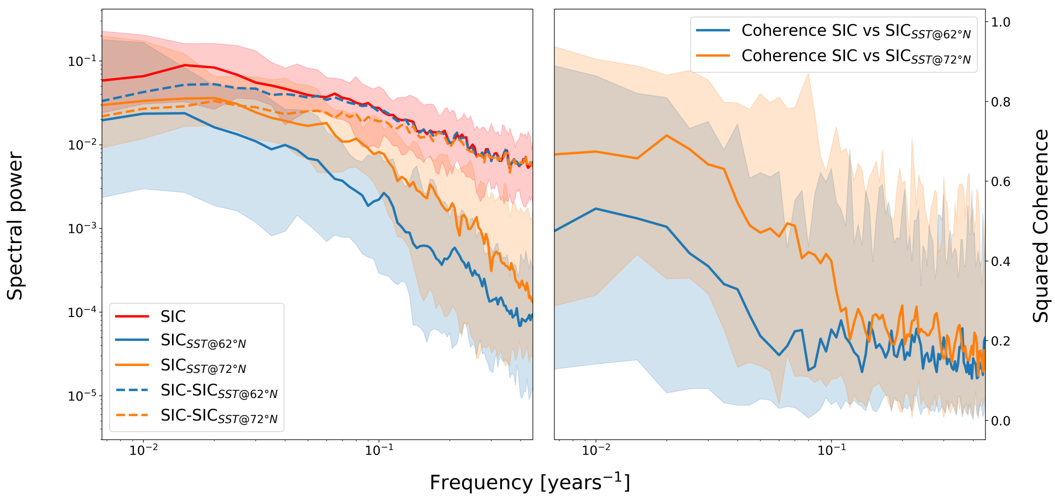

Figure 5. Same as Figure 2, but for the SST based hindcasts. Also, in addition to the full spectra in (a) we show the residual spectra with the dashed lines.

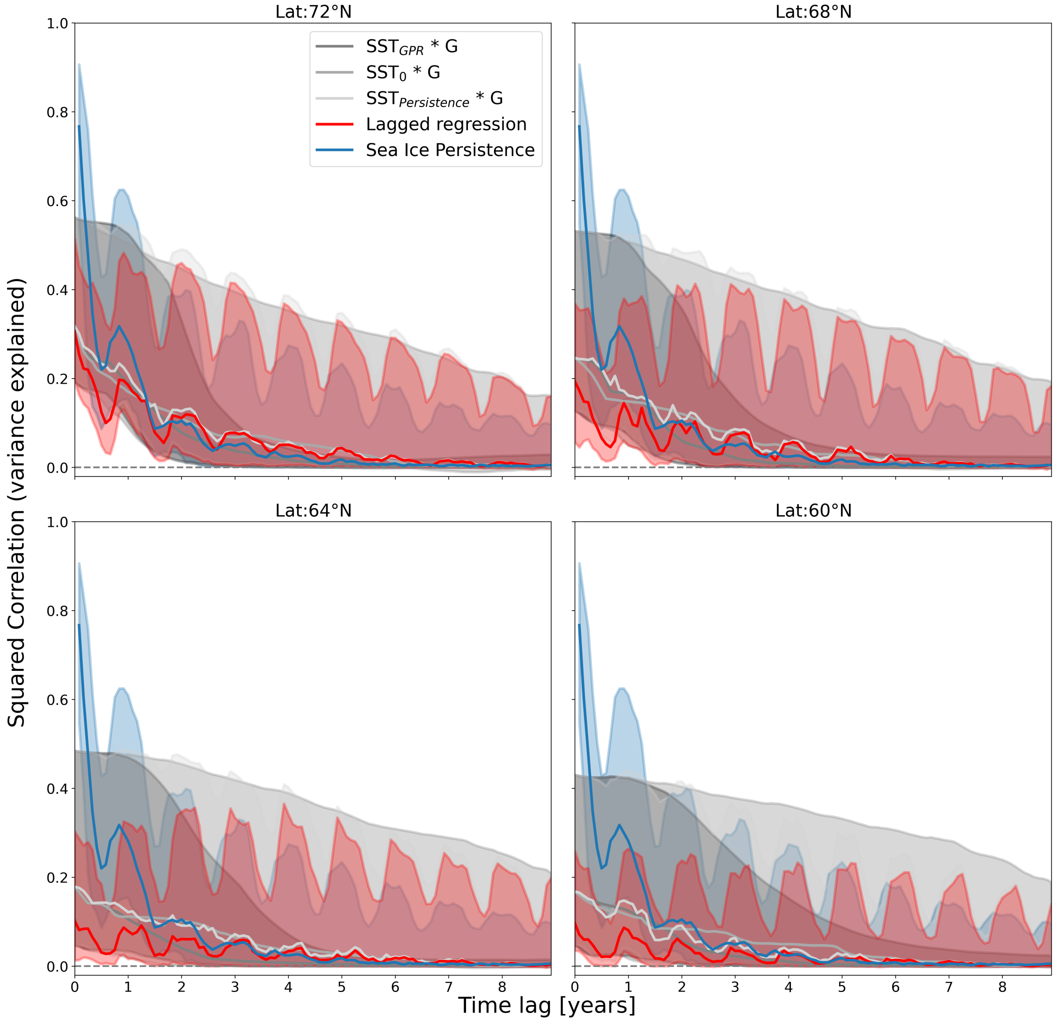

Figure 6. Lagged predictability of the simulated ice cover in CMIP6 models using different measures. Here predictability is measured by squared correlation, but note that the high correlations are due to long-term variability as shown in 4. The solid lines show the median, while the shading shows the 5%-95% range. The different gray lines show the prediction assuming SST anomalies (i) are predicted using a gaussian process model, darkest gray (ii) go to 0 in future lags (iii) persist indefinitely. Red line shows lagged regression at 0 lag and blue shows prediction based on sea ice anomaly persistence.

ocean heat anomalies in the norwegian sea. *Journal of Geophysical Research: Oceans*, *124*(4), 2908-2923. Retrieved from https://agupubs.onlinelibrary.wiley.com/doi/abs/10.1029/2018JC014649 doi: https://doi.org/10.1029/2018JC014649

Bohlinger, P., Breivik, Ø., Economou, T., & Müller, M. (2019). A novel approach to computing super observations for probabilistic wave model validation. *Ocean Modelling*, 101404.

Broomé, S., Chafik, L., & Nilsson, J. (2020). Mechanisms of decadal changes in sea surface height and heat content in the eastern nordic seas. *Ocean Science*, *16*(3), 715–728. Retrieved from https://os.copernicus.org/articles/16/715/2020/ doi: 10.5194/os-16-715-2020

Broomé, S., & Nilsson, J. (2018). Shear dispersion and delayed propagation of temperature anomalies along the norwegian atlantic slope current. *Tellus A: Dynamic Meteorology and Oceanography*, *70*(1), 1-13. Retrieved from https://doi.org/10.1080/16000870.2018.1453215 doi: 10.1080/16000870.2018.1453215

Chafik, L., Nilsson, J., Skagseth, Ø., & Lundberg, P. (2015). On the flow of atlantic water and temperature anomalies in the nordic seas toward the arctic ocean. *Journal of Geophysical Research: Oceans*, *120*(12), 7897-7918. Retrieved from https://agupubs.onlinelibrary.wiley.com/doi/abs/10.1002/2015JC011012 doi: https://doi.org/10.1002/2015JC011012

Chepurin, G. A., & Carton, J. A. (2012). Subarctic and arctic sea surface temperature and its relation to ocean heat content 1982–2010. *Journal of Geophysical Research: Oceans*, *117*(C6). Retrieved from https://agupubs.onlinelibrary.wiley.com/doi/abs/10.1029/2011JC007770 doi: https://doi.org/10.1029/2011JC007770

Cornish, S. B., Kostov, Y., Johnson, H. L., & Lique, C. (2020). Response of arctic freshwater to the arctic oscillation in coupled climate models. *Journal of Climate*, *33*(7), 2533 - 2555. Retrieved from https://journals.ametsoc.org/view/journals/clim/33/7/jcli-d-19-0685.1.xml doi: 10.1175/JCLI-D-19-0685.1

Furevik, T. (2000). On anomalous sea surface temperatures in the nordic seas. *Journal of Climate*, *13*(5), 1044 - 1053. Retrieved from https://journals.ametsoc.org/view/journals/clim/13/5/1520-0442_2000_013_1044_oassti_2.0.co_2.xml doi: 10.1175/1520-0442(2000)013⟨1044:OASSTI⟩2.0.CO;2

Hasselmann, K. (1976). Stochastic climate models part I. Theory. *Tellus*, *28*(6), 473–485.

Helland-Hansen, B., & Nansen, F. (1909). The norwegian sea. its physical oceanography based upon the norwegian researches 1900–1904. *Report on Norwegian Fishery and Marine Investigations*, *2*(2), 1–360.

Jeffress, S. A., & Haine, T. W. N. (2014). Correlated signals and causal transport in ocean circulation. *Quarterly Journal of the Royal Meteorological Society*, *140*(684), 2375-2382. Retrieved from https://rmets.onlinelibrary.wiley.com/doi/abs/10.1002/qj.2313 doi: https://doi.org/10.1002/qj.2313

Johnson, H. L., Cornish, S. B., Kostov, Y., Beer, E., & Lique, C. (2018). Arctic ocean freshwater content and its decadal memory of sea-level pressure. *Geophysical Research Letters*, *45*(10), 4991-5001. Retrieved from https://agupubs.onlinelibrary.wiley.com/doi/abs/10.1029/2017GL076870 doi: 10.1029/2017GL076870

Kostov, Y., Ferreira, D., Armour, K. C., & Marshall, J. (2018). Contributions of greenhouse gas forcing and the southern annular mode to historical southern ocean surface temperature trends. *Geophysical Research Letters*, *45*(2), 1086-1097. Retrieved from https://agupubs.onlinelibrary.wiley.com/doi/abs/10.1002/2017GL074964 doi: https://doi.org/10.1002/2017GL074964

Kostov, Y., Marshall, J., Hausmann, U., Armour, K. C., Ferreira, D., & Holland, M. M. (2017). Fast and slow responses of southern ocean sea surface temperature to sam in coupled climate models. *Climate Dynamics*, *48*, 1595–1609. Retrieved from https://doi.org/10.1007/s00382-016-3162-z doi: 10.1007/s00382-016-3162-z

Lambert, E., Nummelin, A., Pemberton, P., & Ilıcak, M. (2019). Tracing the imprint of river runoff variability on arctic water mass transformation. *Journal of Geophysical Research: Oceans*, *124*(1), 302-319. Retrieved from https://agupubs.onlinelibrary.wiley.com/doi/abs/10.1029/2017JC013704 doi: https://doi.org/10.1029/2017JC013704

Lien, Y., Vidar S.and Gusdal, & Vikebø, F. B. (2014). Along-shelf hydrographic anomalies in the nordic seas (1960–2011): locally generated or advective signals? *Ocean Dynamics*, *64*, 1047–1059. Retrieved from https://doi.org/10.1007/s10236-014-0736-3 doi: 10.1007/s10236-014-0736-3

Muilwijk, M., Smedsrud, L. H., Ilicak, M., & Drange, H. (2018). Atlantic water heat transport variability in the 20th century arctic ocean from a global ocean model and observations. *Journal of Geophysical Research: Oceans*, *123*(11), 8159-8179. Retrieved from https://agupubs.onlinelibrary.wiley.com/doi/abs/10.1029/2018JC014327 doi: https://doi.org/10.1029/2018JC014327

Nilsson, J. (2000). Propagation, diffusion, and decay of sst anomalies beneath an advective atmosphere. *Journal of Physical Oceanography*, *30*(7), 1505 - 1513. Retrieved from https://journals.ametsoc.org/view/journals/phoc/30/7/1520-0485_2000_030_1505_pdados_2.0.co_2.xml doi: 10.1175/1520-0485(2000)030⟨1505:PDADOS⟩2.0.CO;2

Onarheim, I. H., Eldevik, T., Årthun, M., Ingvaldsen, R. B., & Smedsrud, L. H. (2015). Skillful prediction of barents sea ice cover. *Geophysical Research Letters*, *42*(13), 5364-5371. Retrieved from https://agupubs.onlinelibrary.wiley.com/doi/abs/10.1002/2015GL064359 doi: 10.1002/2015GL064359

Pedregosa, F., Varoquaux, G., Gramfort, A., Michel, V., Thirion, B., Grisel, O., ... Duchesnay, E. (2011). Scikit-learn: Machine learning in Python. *Journal of Machine Learning Research*, *12*, 2825–2830.

Rasmussen, C. E., & Williams, C. K. (2006). Gaussian processes for machine learning. 2006. *The MIT Press, Cambridge, MA, USA*, *38*, 715–719.

Reynolds, R. W., Smith, T. M., Liu, C., Chelton, D. B., Casey, K. S., & Schlax, M. G. (2007). Daily high-resolution-blended analyses for sea surface temperature. *Journal of Climate*, *20*(22), 5473 - 5496. Retrieved from https://journals.ametsoc.org/view/journals/clim/20/22/2007jcli1824.1.xml doi: 10.1175/2007JCLI1824.1

Seviour, W. J. M., Codron, F., Doddridge, E. W., Ferreira, D., Gnanadesikan, A., Kelley, M., ... Waugh, D. W. (2019). The southern ocean sea surface temperature response to ozone depletion: A multimodel comparison. *Journal of Climate*, *32*(16), 5107 - 5121. Retrieved from https://journals.ametsoc.org/view/journals/clim/32/16/jcli-d-19-0109.1.xml doi: 10.1175/JCLI-D-19-0109.1

Skagseth, Ø., Furevik, T., Ingvaldsen, R., Loeng, H., Mork, K. A., Orvik, K. A., & Ozhigin, V. (2008). Volume and heat transports to the arctic ocean via the norwegian and barents seas. In R. R. Dickson, J. Meincke, & P. Rhines (Eds.), *Arctic–subarctic ocean fluxes: Defining the role of the northern seas in climate.* Dordrecht: Springer Netherlands. Retrieved from https://doi.org/10.1007/978-1-4020-6774-7_3 doi: 10.1007/978-1-4020-6774-7_3

Sundby, S., & Drinkwater, K. (2007). On the mechanisms behind salinity anomaly signals of the northern north atlantic. *Progress in Oceanography*, *73*(2), 190-202. Retrieved from https://www.sciencedirect.com/science/article/pii/S0079661107000390 doi: https://doi.org/10.1016/j.pocean.2007.02.002

Supporting Information for "Predictability of the Barents Sea ice cover from the sea surface temperatures in a linear framework"

Aleksi Nummelin[1], Chuncheng Guo[1], and Patrik Bohlinger[2]

[1]NORCE Norwegian Research Centre AS and Bjerknes Centre for Climate Research

[2]Norwegian Meteorological Institute

Contents of this file

1. Figures S1 to S2
2. Tables S1

Additional Supporting Information (Files uploaded separately)

1. Captions for large Table S1 (uploaded as separate excel file)

Introduction This supplementary material provides a more detailed view of individual model performance (Fig. S1) as well as multimodel mean response functions for all the months of the year (Fig. S2). We also provide response functions for three models with heat transport output (Fig. S3) as well as table S1 listing all the models used in the analysis.

noindent**Table S1.** List of CMIP6 models and the links to the data on ESGF servers.

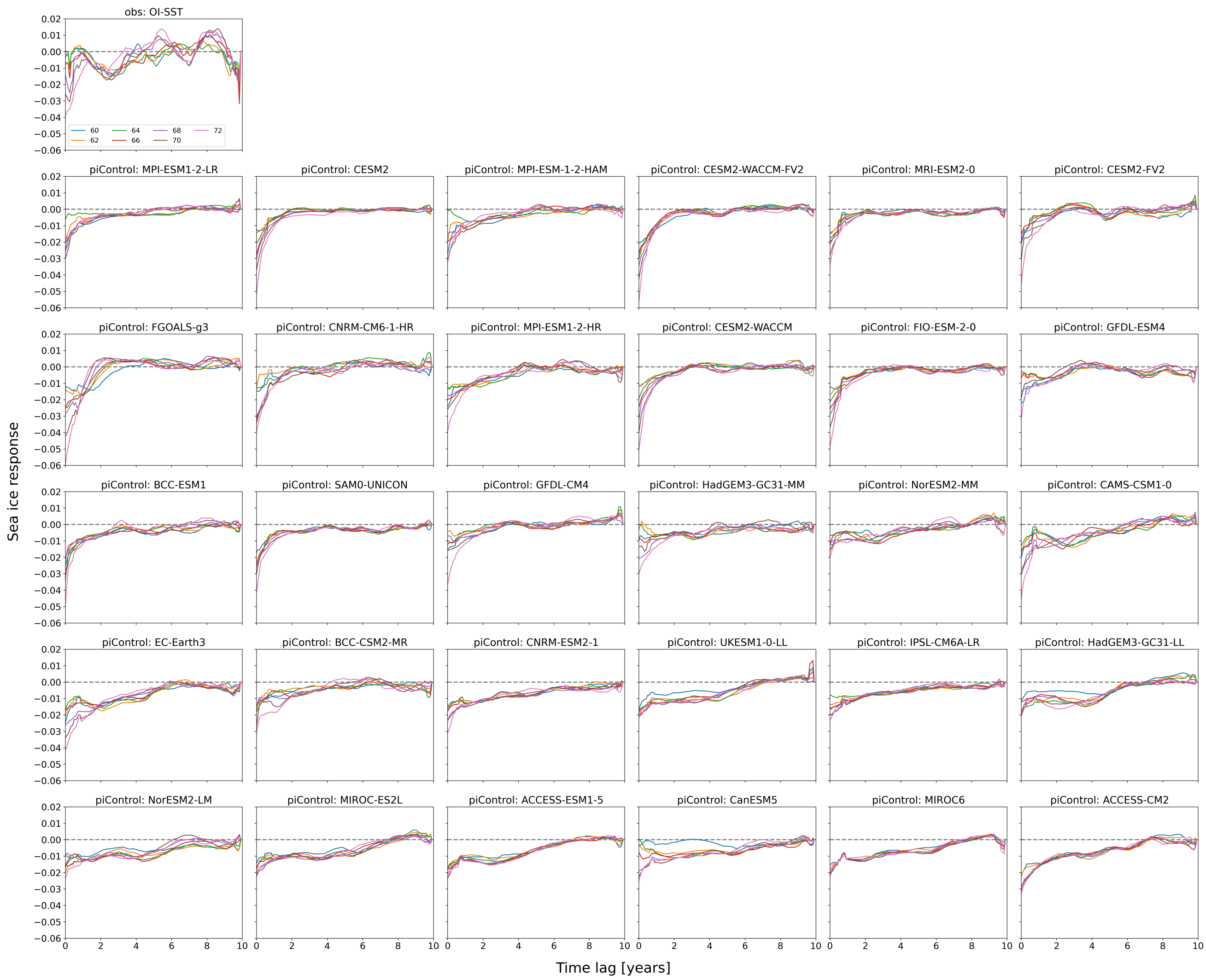

Figure S1. SST response functions for observations and for models (different panels) for different sections (different line colors).

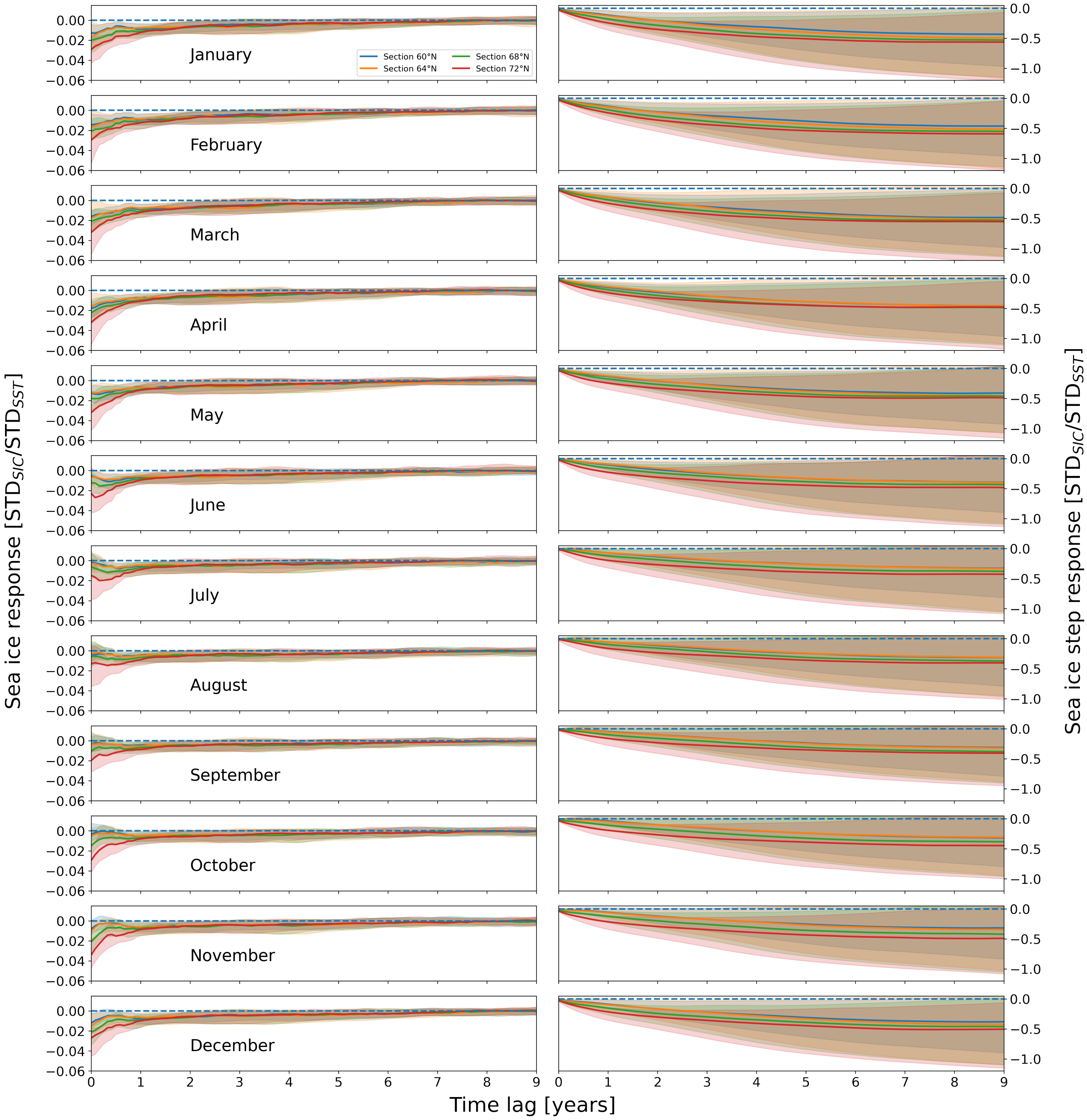

Figure S2. CMIP6 mean sea ice response function in different months, for four SST sections.

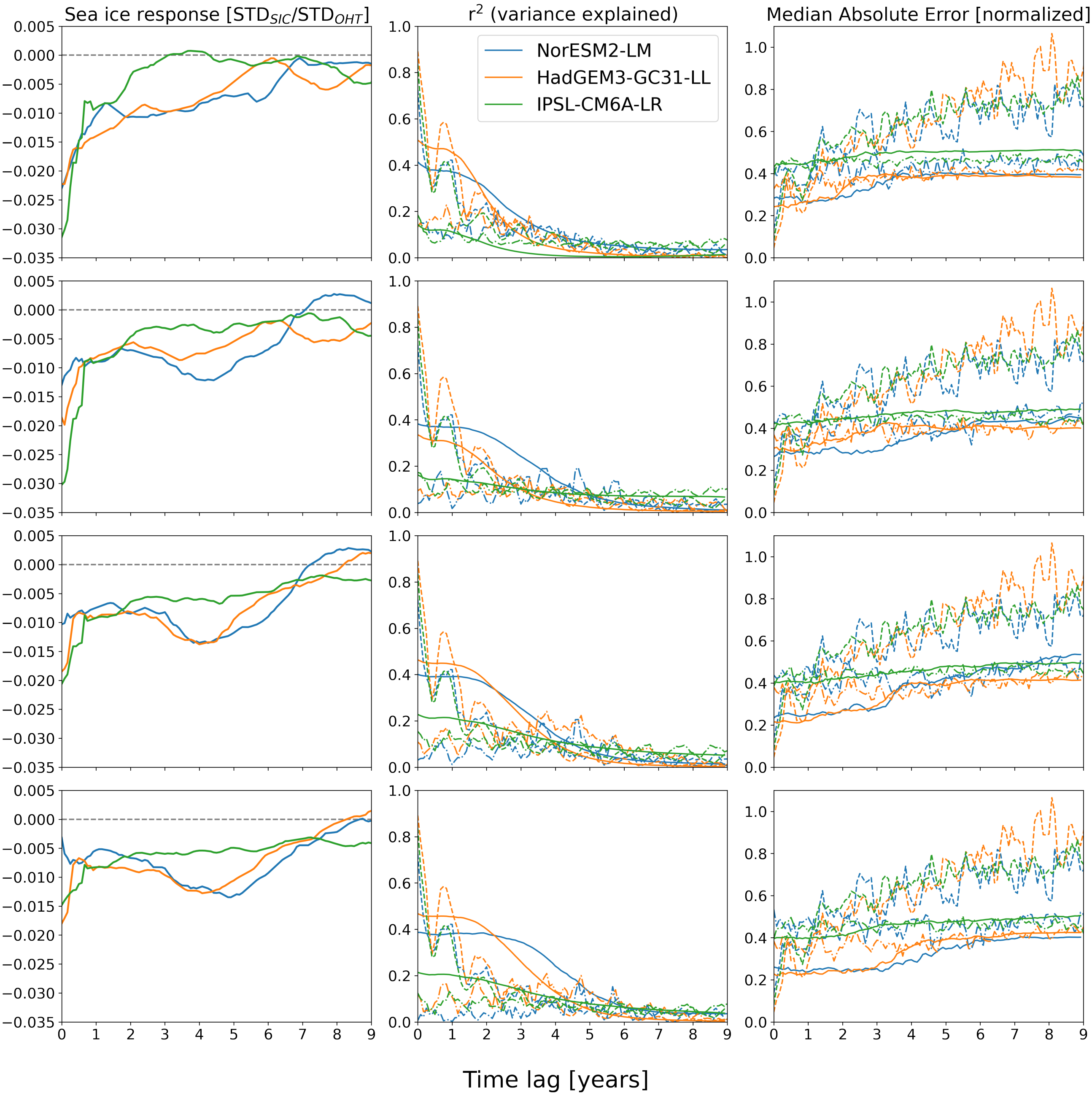

Figure S3. Sea ice response (first column), predictive skill in measured in correlation (second column), predictive skill in measured as mean error (third column). The rows are (from the top) as follows 72N, 68N, 64N, and 60N. The different colors mark the different models, and in the second and third column the different linestyles are as follows: solid line denotes OHT$_{GPR}$·G, dashed-dotted line denotes OHT$_{Persistence}$·G, dashed line denotes sea ice persistence.

Model Name	Institute ID	Ensemble member
ACCESS-CM2	CSIRO-ARCCSS	r1i1p1f1
ACCESS-ESM1-5	CSIRO	r1i1p1f1
BCC-CSM2-MR	BCC	r1i1p1f1
BCC-ESM1	BCC	r1i1p1f1
CAMS-CSM1-0	CAMS	r1i1p1f1
CESM2	NCAR	r1i1p1f1
CESM2-FV2	NCAR	r1i1p1f1
CESM2-WACCM	NCAR	r1i1p1f1
CESM2-WACCM-FV2	NCAR	r1i1p1f1
CNRM-CM6-1-HR	CNRM-CERFACS	r1i1p1f2
CNRM-ESM2-1	CNRM-CERFACS	r1i1p1f1
CanESM5	CCCma	r1i1p1f1
EC-Earth3	EC-Earth-Consortium	r1i1p1f1
FGOALS-g3	CAS	r1i1p1f1
FIO-ESM-2-0	FIO-QLNM	r1i1p1f1
GFDL-CM4	NOAA-GFDL	r1i1p1f1
GFDL-ESM4	NOAA-GFDL	r1i1p1f1
HadGEM3-GC31-LL	MOHC, NERC	r1i1p1f1
HadGEM3-GC31-MM	MOHC	r1i1p1f1
IPSL-CM6A-LR	IPSL	r1i2p1f1
MIROC-ES2L	MIROC	r1i1p1f2
MIROC6	MIROC	r1i1p1f1
MPI-ESM-1-2-HAM	HAMMOZ-Consortium	r1i1p1f1
MPI-ESM-1-2-HR	MPI-M, DWD, DKRZ	r1i1p1f1
MPI-ESM-1-2-LR	MPI-M, AWI	r1i1p1f1
MRI-ESM2-0	MRI	r1i1p1f1
NESM3	NUIST	r1i1p1f1
NorESM2-LM	NCC	r1i1p1f1
NorESM2-MM	NCC	r1i1p1f1
SAM0-UNICON	SNU	r1i1p1f1
UKESM1-0-LL	MOHC, NERC, NIMS-KMA	r1i1p1f2

doi

http://doi.org/10.22033/ESGF/CMIP6.4311
http://doi.org/10.22033/ESGF/CMIP6.4312
http://doi.org/10.22033/ESGF/CMIP6.3016
http://doi.org/10.22033/ESGF/CMIP6.3017
http://doi.org/10.22033/ESGF/CMIP6.9797
http://doi.org/10.22033/ESGF/CMIP6.7733
http://doi.org/10.22033/ESGF/CMIP6.11301
http://doi.org/10.22033/ESGF/CMIP6.10094
http://doi.org/10.22033/ESGF/CMIP6.11302
http://doi.org/10.22033/ESGF/CMIP6.4164
http://doi.org/10.22033/ESGF/CMIP6.4165
http://doi.org/10.22033/ESGF/CMIP6.3673
http://doi.org/10.22033/ESGF/CMIP6.4842
http://doi.org/10.22033/ESGF/CMIP6.3448
http://doi.org/10.22033/ESGF/CMIP6.9205
http://doi.org/10.22033/ESGF/CMIP6.8666
http://doi.org/10.22033/ESGF/CMIP6.8669
http://doi.org/10.22033/ESGF/CMIP6.6294
http://doi.org/10.22033/ESGF/CMIP6.6297
http://doi.org/10.22033/ESGF/CMIP6.5251
http://doi.org/10.22033/ESGF/CMIP6.5710
http://doi.org/10.22033/ESGF/CMIP6.5711
http://doi.org/10.22033/ESGF/CMIP6.5037
http://doi.org/10.22033/ESGF/CMIP6.6674
http://doi.org/10.22033/ESGF/CMIP6.6675
http://doi.org/10.22033/ESGF/CMIP6.6900
http://doi.org/10.22033/ESGF/CMIP6.8776
http://doi.org/10.22033/ESGF/CMIP6.8217
http://doi.org/10.22033/ESGF/CMIP6.8221
http://doi.org/10.22033/ESGF/CMIP6.7791
http://doi.org/10.22033/ESGF/CMIP6.6298